The Astrophysical Journal Letters, 911:L32 (7pp), 2021 April 20 https://doi.org/10.3847/2041-8213/abf491

Velocity Dispersion of the GD-1 Stellar Stream

Megan T. Gialluca[1,2], Rohan P. Naidu[2], and Ana Bonaca[2]
[1] Department of Astronomy and Planetary Science |Northern Arizona University, Box 6010, Flagstaff, AZ 86011, USA; mtg224@nau.edu
[2] Center for Astrophysics | Harvard & Smithsonian, 60 Garden Street, Cambridge, MA 02138, USA
Received 2020 November 25; revised 2021 March 31; accepted 2021 April 1; published 2021 April 26

Abstract

Tidally dissolved globular clusters form thin stellar streams that preserve a historical record of their past evolution. We report a radial velocity dispersion of $2.1 \pm 0.3\,\mathrm{km\,s^{-1}}$ in the GD-1 stellar stream using a sample of 43 spectroscopically confirmed members. The GD-1 velocity dispersion is constant over the surveyed $\approx 15°$ span of the stream. We also measured velocity dispersion in the spur adjacent to the main GD-1 stream, and found a similar value at the tip of the spur. Surprisingly, the region of the spur closer to the stream appears dynamically colder than the main stream. An unperturbed model of the GD-1 stream has a velocity dispersion of $\approx 0.5\,\mathrm{km\,s^{-1}}$, indicating that GD-1 has undergone dynamical heating. Stellar streams arising from globular clusters, which prior to their arrival in the Milky Way, orbited a dwarf galaxy with a cored density profile are expected to have experienced the amount of heating required to match the velocity dispersion observed in GD-1. This suggests that GD-1 has been accreted and that imprints of its original host galaxy, including the inner slope of its dark matter halo, remain observable in the stream today.

Unified Astronomy Thesaurus concepts: Galaxy dynamics (591); Stellar dynamics (1596); Milky Way dynamics (1051); Cold dark matter (265)

1. Introduction

Due to two-body interactions, stars evaporate from globular clusters and form long, thin stellar streams (Spitzer 1987; Combes et al. 1999). Streams that orbit in the Galactic halo can remain coherent for billions of years (Balbinot & Gieles 2018). Intrinsically, they are dynamically cold, so any gravitational anomaly they encounter leaves a record in the distribution of stream stars. Large perturbations, like the passage of a massive dark matter subhalo, typically produce prominent underdensities, or gaps, in a stellar stream (Carlberg 2009; Yoon et al. 2011). Close encounters of less massive objects would predominantly scatter stream stars, thus increasing its thickness and velocity dispersion (Ibata et al. 2002; Johnston et al. 2002).

Excitingly, signatures of dynamical perturbation have recently been detected in the GD-1 stellar stream. Grillmair & Dionatos (2006) discovered GD-1 as a long stellar stream without a progenitor; however, its small width and small spread in metallicity (Bonaca et al. 2020a) signal that GD-1 is a completely dissolved globular cluster. Using proper motions from the Gaia Data Release 2 catalog (Gaia Collaboration et al. 2018) to confidently identify stream member stars, Price-Whelan & Bonaca (2018) discovered large density variations along the GD-1 stream, as well as stars beyond the main stream. These structures were also found using deep photometry alone (de Boer et al. 2018). The origin of these features is unclear, as similar features are produced in simulations of streams that have had a close encounter with a compact, massive object, like a low-mass dark matter subhalo (e.g., Banik et al. 2021; Bonaca et al. 2019), simulations of an unperturbed stream with a much more massive progenitor (e.g., Ibata et al. 2020), and in simulations of stellar streams accreted into the Milky Way from a smaller satellite galaxy (e.g., Malhan et al. 2021).

Velocity dispersion serves as an important indicator of the cumulative amount of perturbation a stream has experienced, and would therefore help to distinguish the relative importance of external and internal processes in shaping the GD-1 stellar stream. Radial velocities are available for a large number of stream member stars distributed over the entire extent of GD-1 (Koposov et al. 2010; Huang et al. 2019), but due to their large measurement uncertainties, they only put an upper limit on the radial velocity dispersion in GD-1 of $\sigma_{V\mathrm{rad}} \leqslant 3\,\mathrm{km\,s^{-1}}$. Using Gaia proper motions, Malhan & Ibata (2019) also put an upper limit on the average tangential velocity dispersion across GD-1 of $\sigma_{V\,\mathrm{tan}} \leqslant 2.3\,\mathrm{km\,s^{-1}}$. Recently, Bonaca et al. (2020a) published a catalog of GD-1 members distributed over a limited range along the stream, but observed with a high-resolution spectrograph so that radial velocity uncertainties are precise enough to resolve a dispersion in radial velocity as low as $\approx 1\,\mathrm{km\,s^{-1}}$.

In this Letter, we first explore how the velocity dispersion of a stellar stream on the GD-1 orbit depends on its age and the progenitor's mass, and estimate the velocity dispersion GD-1 would have in the absence of any perturbations (Section 2). In Section 3 we use radial velocities from Bonaca et al. (2020a) to determine velocity dispersion in GD-1, and show it is significantly larger than predicted by unperturbed models. This suggests that GD-1 has undergone dynamical heating, and in Section 4 we explore plausible heating sources. We work in the GD-1 sky coordinates defined by Koposov et al. (2010), with $\phi_{1,2}$ being the stream longitude and latitude, respectively.

2. Velocity Dispersion in Unperturbed Models of the GD-1 Stream

To determine the velocity dispersion GD-1 would have in the absence of dynamical perturbations, we created a suite of stream models on the GD-1 orbit covering a range of progenitor masses and stream ages. Because the stream is narrow (Price-Whelan & Bonaca 2018), has little dispersion in metallicity (Bonaca et al. 2020a), and has no visible progenitor, we assume the GD-1 progenitor is a completely disrupted globular cluster. We simulate the stream by releasing tracer

particles from the progenitor cluster's tidal radius and evolving them in a Milky Way gravitational potential (the streakline or particle spray method; Bonaca et al. 2014; Fardal et al. 2015). Our Milky Way model includes a Miyamoto & Nagai (1975) disk (mass of $5.5 \times 10^{10}\,M_{\odot}$, scale length of 3 kpc, and scale height of 0.28 kpc), a Hernquist (1990) bulge (mass of $4 \times 10^{9}\,M_{\odot}$, and scale radius of 1 kpc), and a Navarro et al. (1997) dark matter halo (scale mass of $7 \times 10^{11}\,M_{\odot}$, scale radius of 15.62 kpc, and a flattening of 0.95). In our simulations we first create the progenitor's orbit (constrained by Bonaca et al. 2020a to fit the GD-1 stream 6D positions and velocities), and then disperse stars from the progenitor at each simulation time step.

To explore the range of velocity dispersion a stream like GD-1 can attain unperturbed, we simulated models of GD-1 for a range of progenitors' initial masses ($M_{\rm init}$) and stream ages, defined as the time since disruption began until the present (τ). The stream's appearance also depends on the time it took its progenitor to dissolve ($t_{\rm dis}$). We consider two different methods of calculating these dissolution times for a globular cluster on a given orbit. In both cases, the dissolution time depends mainly on the initial mass. Method 1, given by Equation (1), is calibrated empirically using observational data, while Method 2, given by Equation (2), is found through numerical modeling, so in this regard Method 1 would be favorable. However, Method 2 better accounts for GD-1's distance from the Galactic center. We will show that the best-fitting models from both methods have a similar velocity dispersion (within 10%).

In Method 1, the dissolution time is given by:

$$\frac{t_{\rm dis}}{[\rm Myr]} = t_4 \left(\frac{M_{\rm init}}{10^4\,M_{\odot}} \right)^{\gamma}, \tag{1}$$

where t_4 is the disruption time of a $10^4\,M_{\odot}$ globular cluster. We used values of the power-law index $\gamma = 0.62$ and $t_4 = 1$ Gyr, appropriate for clusters dissolving in the inner Milky Way (Boutloukos & Lamers 2003). Because observations of GD-1 show no progenitor, the total disruption time must be shorter than the stream age and so, based on Equation (1), the initial mass cannot exceed $6.6 \times 10^5\,M_{\odot}$ as that would cause the disruption time to be greater than the age of the oldest globular clusters at 13.5 Gyr (Kruijssen et al. 2019) Considering these constraints for Method 1, we ran simulations for progenitor masses of $10\,M_{\odot} - 6.6 \times 10^5\,M_{\odot}$ and for stream ages of 1 Gyr – 13.5 Gyr.

In Method 2, the dissolution time is given by:

$$\frac{t_{\rm dis}}{[\rm Myr]} = \beta \left(\frac{N_{\rm tot}}{\ln(0.02 N_{\rm tot})} \right)^{x} \frac{R_a}{[\rm kpc]} (1 - \epsilon), \tag{2}$$

where β and x are dependent on initial concentration, $N_{\rm tot}$ is the total number of stars in the cluster, R_a is the apocenter distance of GD-1 (given by the modeled orbit), and ϵ is the eccentricity (Baumgardt & Makino 2003). We assume values for β and x of 1.91 and 0.75, respectively, the values of an initial concentration of a $W_0 = 5$ King profile (King 1981) corresponding to the lower concentration of the two cases simulated by Baumgardt & Makino (2003). We calculate $N_{\rm tot}$ using the initial mass function described in Baumgardt & Makino (2003). In general, Method 2 tends to yield higher values of $t_{\rm dis}$ than Method 1; this is because Method 1 has been calibrated closer to the Galactic center, and therefore assumes stronger tidal forces. Thus, the lowest allowed mass when using Equation (2) is $40\,M_{\odot}$ and the lowest allowed age is 1.6 Gyr. In Method 2, the largest allowed age is $1.3 \times 10^4\,M_{\odot}$ as masses above this return dissolution times larger than 13.5 Gyr. Considering the constraints for Method 2, we ran simulations for progenitor masses of $40\,M_{\odot} - 1.3 \times 10^4\,M_{\odot}$ and for stream ages of 1.6–13.5 Gyr.

Figure 1 shows a summary of all simulations we ran. The first two rows show models employing Method 1, and the last two rows show those using Method 2 to estimate the dissolution time. For each simulated model we calculated how well it reproduces the extent of the observed GD-1 stream. The first and third rows of Figure 1 show the χ^2 values for each given model as a function of initial progenitor mass and total stream age since disruption began. To calculate χ^2, we compare the 5th and 95th percentiles of the ϕ_1 coordinates for the current model and the stream track from Price-Whelan & Bonaca (2018); in this calculation we assume a model uncertainty of 2°. Our χ^2 treatment is given by:

$$\chi^2 = \frac{(\phi_{95,M} - \phi_{95,\rm ST})^2 + (\phi_{5,M} - \phi_{5,\rm ST})^2}{\sigma^2}, \tag{3}$$

where $\phi_{95,M}$ and $\phi_{5,M}$ are the 95th and 5th percentiles of the ϕ_1 values of our model and $\phi_{95,\rm ST}$ and $\phi_{5,\rm ST}$ are the 95th and 5th percentiles of the ϕ_1 values of the identified stream track. σ is the model uncertainty (2°). By using this χ^2 treatment we are effectively considering the stream length as a quantifier for agreement between our model and the stream track. This could be improved upon in the future by considering other factors, such as the stream width, but it is sufficient for us to estimate the velocity dispersion of an unperturbed GD-1. The subtle zigzag pattern in the top leftmost plot has spacings between peaks comparable to that of GD-1's orbital period, thus we expect this unusual pattern to be a result of periodic stretching of the stream along its orbit. As expected, the progenitor masses and stream ages of models that reproduce the GD-1 length well are anticorrelated in both methods.

The second and last rows of Figure 1 show the velocity dispersion ($\sigma_{\rm Vrad}$) as a function of initial progenitor mass ($\rm M_{init}$) and total stream age since disruption began (τ). When calculating the velocity dispersion, we consider radial velocities relative to the orbital radial velocity, $\Delta V_{\rm rad} = V_{\rm rad} - V_{\rm rad,orbit}$, where $V_{\rm rad}$ is the stream radial velocity, and $V_{\rm rad,orbit}$ is the orbital radial velocity derived as a function of the stream longitude. We report velocity dispersion of simulated streams in the same region of the sky where precise measurements of radial velocities are available. The stream velocity dispersion increases with increasing mass and age, with mass being the more influential parameter. Overall, our models have a low dispersion ($\lesssim 2\ \rm km\ s^{-1}$), so we expect that, with no external perturbations, a stream like GD-1 should be very cold dynamically.

The first column of Figure 1 presents the wide range of models we ran. However, some combinations of the initial mass and stream age are missing because they produce streams inconsistent with the observed GD-1. For low-mass and small age runs, the streams are too short to populate the range of $\phi_{1,2}$ where we have observational data on GD-1 radial velocities, meaning there is no velocity dispersion to compare to in this

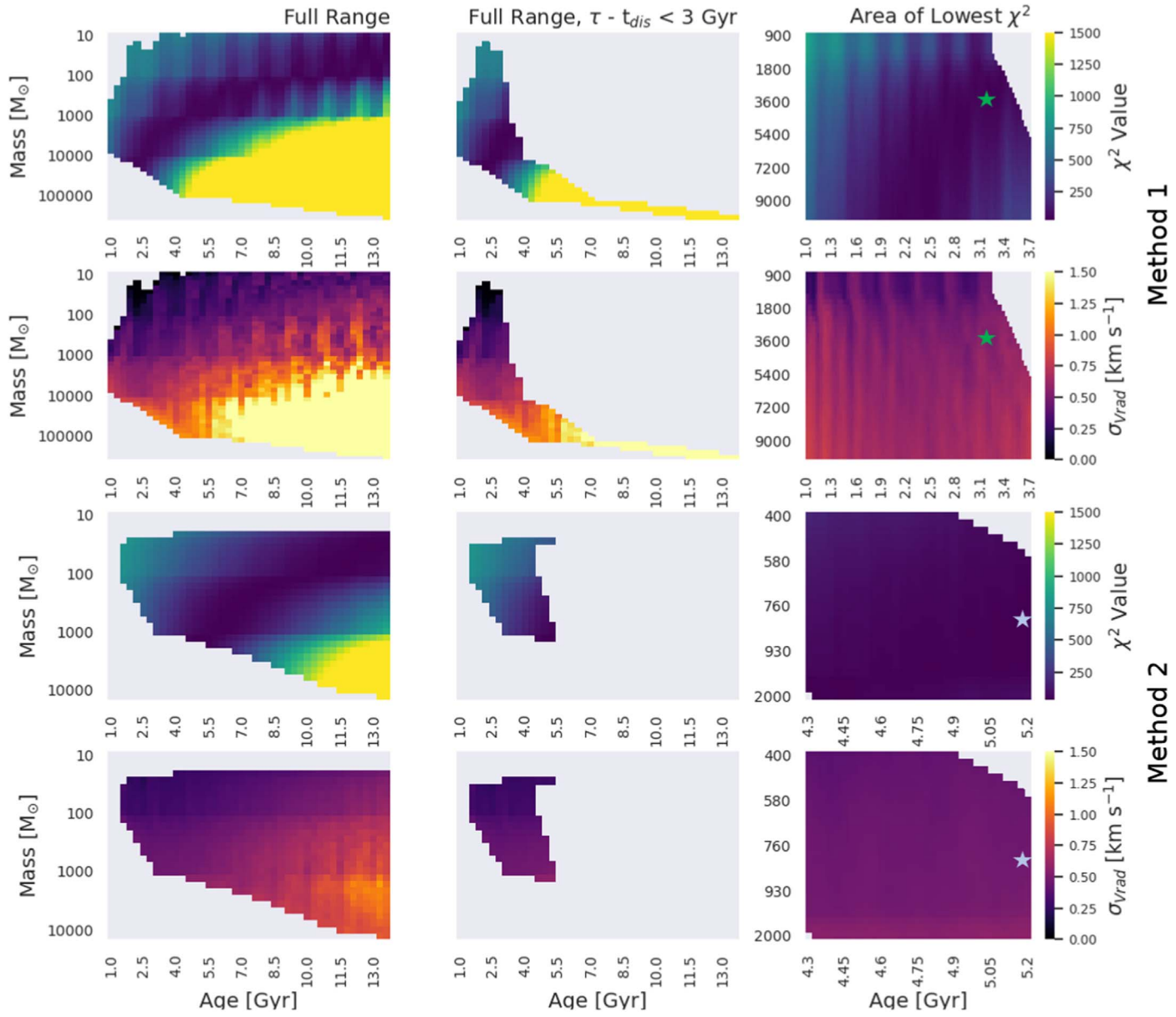

Figure 1. Summary of all simulations of the GD-1 stellar stream. The top two rows employ an empirical method for estimating the progenitor's dissolution time (Method 1), while the bottom two rows employ a theoretically derived relation (Method 2). χ^2 values for each model in comparison to the observed stream track as a function of the initial mass and stream age are shown in rows 1 and 3. Velocity dispersions of each model as a function of the initial progenitor mass and total stream age since disruption began are shown in rows 2 and 4. Left column: full range of models. Middle column: models in which the difference between the stream age and dissolution time is smaller than 3 Gyr. Right column: a refined grid around the lowest χ^2 regions. The best-fit models are denoted with green and light blue stars for Methods 1 and 2, respectively.

area. For high mass and small age runs, the progenitor survives to the present, unlike the observed GD-1 with no discernible progenitor.

To further narrow down plausible models of GD-1, in the second column of Figure 1 we only show models whose progenitors disrupted within the last 3 Gyr, i.e., $\tau - t_{\rm dis} < 3$ Gyr. As streams phase-mix rapidly following complete dissolution of the progenitor (Helmi & White 1999), we expect older models to be much more diffuse than the observed GD-1. In order to find the best-fitting model, the third column of Figure 1 shows a larger suite of models within the lowest χ^2 range, identified in the second column. For Method 1, column three uses 41 evenly spaced mass points in log space from 900 $M_\odot$ to 30, 000 $M_\odot$ and 91 linearly spaced age points from 1 Gyr to 3.7 Gyr. For Method 2, column three uses 25 evenly spaced mass points in log space from 400 $M_\odot$ to 2000 $M_\odot$ and 31 linearly spaced age points from 4.3 Gyr to 5.2 Gyr. Our best-fit model for Method 1 yields a velocity dispersion ($\sigma_{\rm Vrad,model}$) of 0.52 km s^{-1} while the best-fit model for Method 2 yields a velocity dispersion of 0.48 km s^{-1}. Since these values are within 10%, and the best-fit model for Method 1 better matches the extent of the stream, we will proceed with Method 1 for the remainder of the paper.

Our fiducial model has an initial progenitor mass of $3.3 \times 10^3\, M_\odot$, a total stream age of 3.19 Gyr, and a time since total progenitor disruption ($\tau - t_{\rm dis}$) of 2.716 Gyr. The sky positions of the model are shown with green points in the top panel of Figure 2. Our best-fit model matches well the observed

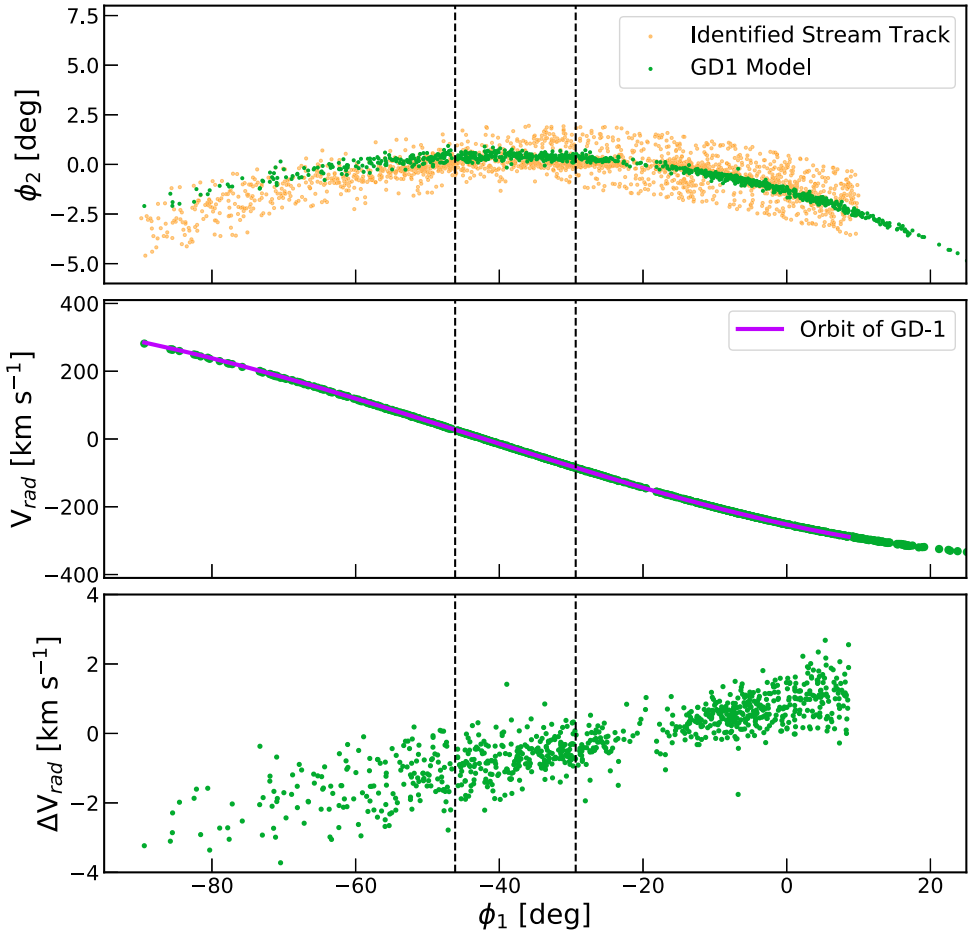

Figure 2. Top: sky positions of our fiducial GD-1 stream model that matches the extent of the observed stream (in the stream coordinates with longitude ϕ_1 and latitude ϕ_2). Middle: radial velocity, $V_{\rm rad}$, along the stream. The purple line shows the orbital radial velocity of the modeled GD-1, $V_{\rm rad,orb}$. Bottom: relative radial velocity of the modeled stream with respect to the orbital radial velocity, $\Delta V_{\rm rad} = V_{\rm rad} - V_{\rm rad,orb}$. We analyzed the model between dashed black lines, which enclose the region where high-resolution spectroscopy is available for GD-1 stars.

extent of the GD-1 stream, as identified by Price-Whelan & Bonaca (2018; orange points).

The simulated stream shows a strong radial velocity gradient (Figure 2, middle panel), which is well described by the orbital radial velocity ($V_{\rm rad,orbit}$, purple line). Radial velocity relative to the orbital, $\Delta V_{\rm rad}$, shows that the stream is kinematically cold (Figure 2, bottom panel). In the region where precise velocities are available observationally ($-46^\circ \leqslant \phi_1 \leqslant -29^\circ$, denoted by black dotted vertical lines in Figure 2), the best-fit unperturbed model of the GD-1 stellar stream has an average velocity dispersion of $\sigma_{\rm Vrad,Model} = 0.52\,{\rm km\,s^{-1}}$. In general, the velocity dispersion increases with distance from the center of the stream; however, the change in this narrow region of the stream is negligible, so for simplicity we only calculate the average value. Our best-fit model is comparable to the results presented in Webb & Bovy (2019) and found through more realistic N-body modeling. In particular, their best-fit model has a velocity dispersion within 10% of the value in our best-fit model (J. Webb, 2020, private communication).

3. Measured Velocity Dispersion in GD-1

We use precise radial velocities of 43 dynamically and chemically identified GD-1 members from Bonaca et al. (2020a) to measure the stream's velocity dispersion. The top panel of Figure 3 shows the sky locations of these stars in the GD-1 coordinate system defined by Koposov et al. (2010). Our sample contains stars located both in the main GD-1 stream (green points) and in the spur (purple points). The observed radial velocities show a strong gradient along the stream, driven by the orbital velocity trend.

We assume that the relative radial velocities, $\Delta V_{\rm rad,i}$ are normally distributed around the best-fit orbit (parameterized by μ), and that both the observational uncertainties, σ_i, and the stream velocity dispersion, $\sigma_{\rm Vrad}$, contribute to the overall dispersion, Σ, such that $\Sigma^2 = (2\sigma_i)^2 + \sigma^2_{\rm Vrad}$. The factor of 2 accounts for systematic uncertainty in the observations (from, e.g., binarity) and is informed by the repeat radial velocity observations of Conroy et al. (2019) in their H3 Spectroscopic Survey of the halo that uses the same instrument in the exact same setting that the data at hand were acquired with, as well as the same data reduction and analysis pipeline. We also note that repeat RV measurements for stream stars from the S5 Survey (Li et al. 2019)—the most apt comparison for this work—are very well modeled by a Gaussian of width $1\sigma_i$, indicating a level of systematic uncertainty from phenomena like binarity that is accounted for in our $2\times$ inflation of σ_i. This empirical argument around binarity resembles those discussed in the context of low-mass dwarfs and clusters (e.g., Simon & Geha 2007; McConnachie & Côté 2010; Cottaar et al. 2012). Nonetheless, repeat observations of GD1 would be very

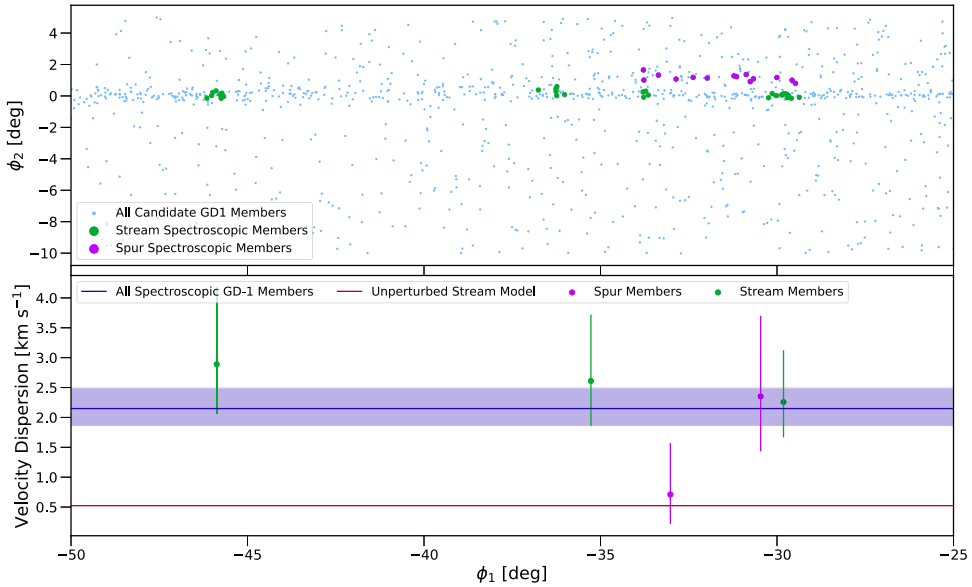

Figure 3. Top: sky positions of likely GD-1 stars (light blue points), and spectroscopically confirmed members in the main stream (green) and in the spur (purple). Bottom: velocity dispersion along the GD-1 stream. Velocity dispersion measured in GD-1 overall (dark blue shaded region) is significantly higher than expected for an unperturbed stream on this orbit (dark red line, see Section 2).

valuable to pin down the exact binary fraction and we defer this to future work.

The probability of relative radial velocity of a star i given the mean radial velocity offset and dispersion is:

$$p_i(\Delta V_{\rm rad,i}|\mu, \Sigma) = \mathcal{N}(\Delta V_{\rm rad,i}|\mu, \Sigma). \quad (4)$$

Assuming that the radial velocity measurements of individual stars are independent, the joint likelihood is simply $p(\{\Delta V_{\rm rad}\}|\mu, \Sigma) = \prod_i \mathcal{N}(\Delta V_{\rm rad,i}|\mu, \Sigma)$. We measured the posterior distribution of the mean relative radial velocity and dispersion in GD-1 by sampling this likelihood using the affine invariant Markov Chain Monte Carlo ensemble sampler *emcee* (Foreman-Mackey et al. 2013). We advanced 200 walkers for 2500 steps, and analyzed the converged chains after discarding the first 500 burn-in steps. Posterior distributions of the relative radial velocity and velocity dispersion for the GD-1 stream overall are shown in Figure 4. As expected, the relative offset of radial velocity measurements from the best-fit orbit is small and consistent with zero. The stream dispersion, however, is well resolved at $\sigma_{\rm Vrad} = 2.1 \pm 0.3\,{\rm km\,s^{-1}}$, which is considerably larger than expected for an unperturbed GD-1 stream (see Section 2).

The bottom panel of Figure 3 shows velocity dispersion along the GD-1 stream. Our sample contains stars observed in eight fields, some of which have only a handful of member stars. To mitigate the effect of small sample size on the estimate of the stream's velocity dispersion, adjacent low-density fields have been combined so that every measurement is based on at least 6 stars. With the exception of an extremely cold spur field at $\phi_1 \approx -33°$, which has a low dispersion of $\sigma \lesssim 1\,{\rm km\,s^{-1}}$, velocity dispersion in the observed stream region is remarkably constant at $\sigma \approx 2.5\,{\rm km\,s^{-1}}$.

4. Summary and Discussion

We measured the average radial velocity dispersion of $\sigma_{\rm Vrad} = 2.1 \pm 0.3\,{\rm km\,s^{-1}}$ in a region of the GD-1 stellar stream

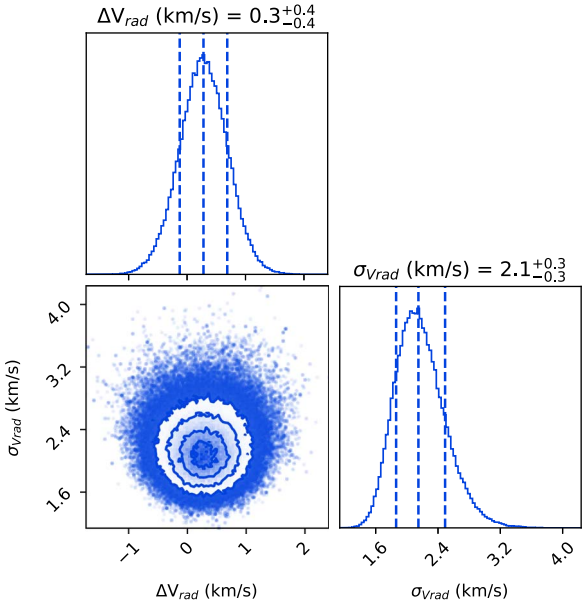

Figure 4. Posterior probability distributions of the relative radial velocity ($\Delta V_{\rm rad}$) with respect to the stream's orbit and the stream's velocity dispersion ($\sigma_{\rm Vrad}$) constrained by all GD-1 member stars.

that contains the adjacent spur ($-46° \lesssim \phi_1 \lesssim -29°$). Velocity dispersion is approximately constant along this part of the stream, except in the inner part of the spur, which is somewhat colder than the average. We produced a fiducial numerical model of the GD-1 stream and found that unperturbed, it has a velocity dispersion of $\sigma_{\rm Vrad,Model} = 0.52\,{\rm km\,s^{-1}}$. On a given orbit, dispersion is larger for older streams and for streams with more massive progenitors. However, to match the observed velocity dispersion, we would need an unrealistically massive progenitor and dynamically old stream. Therefore, the observed velocity dispersion implies GD-1 has been dynamically heated.

The morphology of the gap and the spur observed in the GD-1 stream can be reproduced by numerical models of the stream interacting with a massive object in the Milky Way halo

(Bonaca et al. 2019; de Boer et al. 2020), and the interaction might have elevated the stream's velocity dispersion. However, similarly high values of velocity dispersion were measured in the Palomar 5 tidal tails ($\sigma = 2.1 \pm 0.4\,\mathrm{km\,s^{-1}}$; Kuzma et al. 2015) and the ATLAS-Aliqa Uma complex ($\sigma = 4.8 \pm 0.4\,\mathrm{km\,s^{-1}}$, Li et al. 2020). This motivates us to explore stream heating mechanisms that can affect many streams globally.

4.1. Fuzzy Dark Matter Heating

When simulating stellar streams, we represented the Milky Way's dark matter halo as a spatially smooth, analytic density distribution. However, most models of dark matter predict that dark matter halos have at least some amount of substructure (Bode et al. 2001; Springel et al. 2008). In the case of cold dark matter, low-mass subhalos orbiting within the Milky Way would heat streams like GD-1 (e.g., Ibata et al. 2002; Johnston et al. 2002). As these subhalos have yet to be detected, dark matter models that severely suppress substructure on small scales have been proposed. Fuzzy dark matter is one such model where dark matter is an ultra-light axion of mass $\approx 10^{-22}$ eV (Hu et al. 2000). Due to the low particle mass, fuzzy dark matter exhibits quantum effects on astrophysical scales, including fluctuations in the local density of dark matter. Numerical simulations show that this quantum turbulence can dynamically heat stellar streams (Amorisco & Loeb 2018), as well as field stars (Church et al. 2019). Here we test whether fuzzy dark matter heating can explain the velocity dispersion observed in GD-1.

Following Amorisco & Loeb (2018), we assume that the fuzzy dark matter fluctuations can be modeled as a population of soliton clumps whose density is given by the local dark matter density, and whose size, $r_{\rm sc}$, increases for decreasing axion mass: $r_{\rm sc} = r_{\rm sc,1}/m_{22}$, where $m_{\rm FDM} = m_{22} \times 10^{-22}$ eV is the axion mass and $r_{\rm sc,1} = 0.2$ kpc the soliton radius appropriate for the Milky Way halo. In our model of the Milky Way, average dark matter density along the GD-1 orbit is $\rho = 4.2 \times 10^6\,M_\odot\,\mathrm{kpc^{-3}}$. So, the effective mass of soliton clumps that GD-1 encounters is:

$$M_{\rm eff} = 4\pi/3\; r_{\rm sc}^3\; \rho = 1.4 \times 10^5 m_{22}^{-3}\; M_\odot. \tag{5}$$

As expected, for lighter axion particles the effective mass of soliton clumps increases and so does dynamical heating due to fuzzy dark matter turbulence.

Encounter with a soliton clump imparts a velocity kick to stream stars. Averaged over time, these velocity kicks increase the stream's velocity dispersion. Hui et al. (2017) derived an expression for the velocity dispersion increase as a function of the perturbers' mass, size, and number density (Equation (48)), which we integrate over time to obtain cumulative velocity dispersion due to soliton clump heating:

$$\sigma_{\rm FDM}^2 = \frac{4\pi (kGM_{\rm eff}\,w)^2 N\tau}{V r_{\rm sc}^2}, \tag{6}$$

where $N = 1/V_{\rm sc} = 3/(4\pi) r_{\rm sc}^{-3}$ is the number density of clumps, V is the soliton speed relative to the stream, w is the stream width, τ is its age, G is the gravitational constant, and k is a geometric factor. For simplicity, we assume $k = 1$ (appropriate if soliton clumps were point masses). Substituting definitions for the effective mass and size of soliton clumps in Equation (6), we obtain the following expression for the axion mass as a function of stream velocity dispersion:

$$m_{\rm FDM} = \frac{3\tau\,(Gw\;1.4 \times 10^5\,M_\odot)^2}{V\sigma_{\rm FDM}^2 r_{sc,1}^5} \times 10^{-22}\,\mathrm{eV}. \tag{7}$$

As found by Amorisco & Loeb (2018), dynamically hotter streams imply lighter fuzzy dark matter particles.

Assuming that the velocity dispersion we observed in GD-1 is entirely due to fuzzy dark matter heating, i.e., $\sigma_{\rm FDM} = \sigma_{\rm Vrad} = 2.1\,\mathrm{km\,s^{-1}}$, the solitons are moving at typical speeds of $V = 220\,\mathrm{km\,s^{-1}}$, adopting the stream age from our fiducial model $\tau = 3.19$ Gyr, and taking the stream width from the literature ($w = \mathrm{FWHM} = 0.^\circ 5$, or 80 pc at 10 kpc Koposov et al. 2010), we find $m_{\rm FDM} = 7.7^{+2.6}_{-2.0} \times 10^{-24}$ eV. To take into account that unperturbed stellar streams have nonzero velocity dispersion, we next assume that the GD-1 velocity dispersion due to fuzzy dark matter heating is $\sigma_{\rm FDM} = \sqrt{\sigma_{\rm Vrad}^2 - \sigma_{\rm Vrad,Model}^2} = 1.58\,\mathrm{km\,s^{-1}}$, where $\sigma_{\rm Vrad}$ is the measured velocity dispersion (Section 3), and $\sigma_{\rm Vrad,model}$ is the velocity dispersion in the unperturbed GD-1 model (Section 2), yielding only a slightly more massive estimate $m_{\rm FDM} = 8.2^{+3.0}_{-2.2} \times 10^{-24}$ eV. Fuzzy dark matter particles from this light have been ruled out by the population of low-mass dwarf galaxies in the Milky Way ($m_{\rm FDM} > 2.9 \times 10^{-21}$ eV; Nadler et al. 2021). Heating from the allowed fuzzy dark matter models is insufficient to produce velocity dispersion measured in this part of the GD-1 stellar stream.

4.2. Progenitor Galaxy Heating

One important piece of context is that GD-1 likely arrived with a dwarf galaxy. In recent years the stellar halo, and a number of halo globular clusters, have been shown to arise almost entirely out of accretion (Massari et al. 2019; Naidu et al. 2020). This accretion origin likely also holds for disrupted globular clusters like GD-1. Locating the host dwarf galaxy of GD-1 and dating its accretion redshift, through, e.g., ages of its main-sequence stars (Bonaca et al. 2020b), or dynamical arguments (Koppelman et al. 2019), would further clarify the origin of the stream.

Understanding this origin is important, since GD-1 may have undergone some degree of processing in its accreted host galaxy prior to falling into the Milky Way, adding to its present day observed velocity dispersion (Carlberg 2018, 2020). Following the disruption of globular clusters that were accreted into the Milky Way with a dwarf galaxy, Malhan et al. (2021) found that the velocity dispersion of the resulting streams depends on the dark matter density profile of their original host galaxies. For cuspy dwarf galaxy hosts, the stream velocity dispersion is expected in the range of $\sigma_{\rm Vrad} \approx 5 - 10\,\mathrm{km\,s^{-1}}$, significantly higher than that of GD-1. However, cored dwarfs are less disruptive to their globular clusters, and as a result their streams are colder with $\sigma_{\rm Vrad} \approx 2 - 3\,\mathrm{km\,s^{-1}}$. The radial velocity dispersion we measured in GD-1 can be explained by the GD-1 progenitor cluster having been accreted in a cored dwarf galaxy.

While tantalizing, the accretion origin of the GD-1 stream is still a preliminary finding. In this work we only measured radial velocities in a fraction of the stream, which may have an elevated dispersion due to a local perturbation (e.g., one that produced the stream's gap and spur). Similarly precise measurements across the entire stream are required to establish whether the velocity dispersion is globally high, as expected if

GD-1 were accreted. Independently, tidal debris of the host galaxy should be identifiable as a broader structure on similar orbits in the Galactic halo, whose velocity dispersion is also sensitive to the inner slope of dark matter density (Errani et al. 2015).

Our study of velocity dispersion in the GD-1 stellar stream is a teaser of what will soon be possible in many streams. Massive spectroscopic surveys like SDSS-V (Kollmeier et al. 2017) and DESI (DESI Collaboration et al. 2016) are slated to deliver millions of stellar spectra. Similar analyses of these data will allow us to measure structural properties in a population of dissolved Milky Way progenitors and test dark matter models through velocity dispersions of stellar streams orbiting in the Galactic halo.

We thank the referee for valuable feedback and suggestions. We also thank Eduardo Balbinot and Jeremy Webb for helpful feedback on binarity and numerical models of GD-1, respectively. We would also like to acknowledge Dr. Matthew Ashby and Dr. Jonathan McDowell for their guidance, assistance, and support. We further thank Ali Kurmus, Diana Khimey, Victoria Ono, and Sownak Bose for valuable feedback and support during the summer group meetings. This work was started during the 2020 SAO Summer Astrophysics REU Program. The SAO REU program is funded in part by the National Science Foundation REU and Department of Defense ASSURE programs under NSF Grant no. AST-1852268, and by the Smithsonian Institution. M.G. acknowledges support from the Goldwater Scholarship. A.B. acknowledges support from NASA through HST grant HST-GO-15930.

Software: *Astropy* (Astropy Collaboration et al. 2013; Price-Whelan et al. 2018), *emcee* (Foreman-Mackey et al. 2013), *gala* (Price-Whelan 2017), *matplotlib* (Hunter 2007), *numpy* (Walt et al. 2011), *scipy* (Virtanen et al. 2020).

ORCID iDs

Megan T. Gialluca https://orcid.org/0000-0002-2587-0841
Rohan P. Naidu https://orcid.org/0000-0003-3997-5705
Ana Bonaca https://orcid.org/0000-0002-7846-9787

References

Amorisco, N. C., & Loeb, A. 2018, arXiv:1808.00464
Astropy Collaboration, Robitaille, T. P., Tollerud, E. J., et al. 2013, A&A, 558, A33
Balbinot, E., & Gieles, M. 2018, MNRAS, 474, 2479
Banik, N., Bovy, J., Bertone, G., Erkal, D., & de Boer, T. J. L. 2021, MNRAS, 502, 2364
Baumgardt, H., & Makino, J. 2003, MNRAS, 340, 227
Bode, P., Ostriker, J. P., & Turok, N. 2001, ApJ, 556, 93
Bonaca, A., Conroy, C., Cargile, P. A., et al. 2020b, ApJL, 897, L18
Bonaca, A., Conroy, C., Hogg, D. W., et al. 2020a, ApJL, 892, L37
Bonaca, A., Geha, M., Küpper, A. H. W., et al. 2014, ApJ, 795, 94
Bonaca, A., Hogg, D. W., Price-Whelan, A. M., & Conroy, C. 2019, ApJ, 880, 38
Boutloukos, S., & Lamers, H. 2003, MNRAS, 338, 717
Carlberg, R. G. 2009, ApJL, 705, L223
Carlberg, R. G. 2018, ApJ, 861, 69
Carlberg, R. G. 2020, ApJ, 889, 107
Church, B. V., Mocz, P., & Ostriker, J. P. 2019, MNRAS, 485, 2861
Combes, F., Leon, S., & Meylan, G. 1999, A&A, 352, 149
Conroy, C., Bonaca, A., Cargile, P., et al. 2019, ApJ, 883, 107
Cottaar, M., Meyer, M. R., & Parker, R. J. 2012, A&A, 547, A35
de Boer, T. J. L., Belokurov, V., Koposov, S. E., et al. 2018, MNRAS, 477, 1893
de Boer, T. J. L., Erkal, D., & Gieles, M. 2020, MNRAS, 494, 5315
DESI Collaboration, Aghamousa, A., Aguilar, J., et al. 2016, arXiv:1611.00036
Errani, R., Penarrubia, J., & Tormen, G. 2015, MNRAS, 449, L46
Fardal, M. A., Huang, S., & Weinberg, M. D. 2015, MNRAS, 452, 301
Foreman-Mackey, D., Hogg, D. W., Lang, D., & Goodman, J. 2013, PASP, 125, 306
Gaia Collaboration, Brown, A. G. A., Vallenari, A., et al. 2018, A&A, 616, A1
Grillmair, C. J., & Dionatos, O. 2006, ApJL, 643, L17
Helmi, A., & White, S. D. M. 1999, MNRAS, 307, 495
Hernquist, L. 1990, ApJ, 356, 359
Hu, W., Barkana, R., & Gruzinov, A. 2000, PhRvL, 85, 1158
Huang, Y., Chen, B. Q., Zhang, H. W., et al. 2019, ApJ, 877, 13
Hui, L., Ostriker, J. P., Tremaine, S., & Witten, E. 2017, PhRvD, 95, 043541
Hunter, J. D. 2007, CSE, 9, 90
Ibata, R., Thomas, G., Famaey, B., et al. 2020, ApJ, 891, 161
Ibata, R. A., Lewis, G. F., Irwin, M. J., & Quinn, T. 2002, MNRAS, 332, 915
Johnston, K. V., Spergel, D. N., & Haydn, C. 2002, ApJ, 570, 656
King, I. 1981, QJRAS, 22, 227
Kollmeier, J. A., Zasowski, G., Rix, H.-W., et al. 2017, arXiv:1711.03234
Koposov, S. E., Rix, H.-W., & Hogg, D. W. 2010, ApJ, 712, 260
Koppelman, H. H., Helmi, A., Massari, D., Price-Whelan, A. M., & Starkenburg, T. K. 2019, A&A, 631, L9
Kruijssen, J. M. D., Pfeffer, J. L., Reina-Campos, M., Crain, R. A., & Bastian, N. 2019, MNRAS, 486, 3180
Kuzma, P. B., Da Costa, G. S., Keller, S. C., & Maunder, E. 2015, MNRAS, 446, 3297
Li, T. S., Koposov, S. E., Erkal, D., et al. 2020, arXiv:2006.10763
Li, T. S., Koposov, S. E., Zucker, D. B., et al. 2019, MNRAS, 490, 3508
Malhan, K., & Ibata, R. A. 2019, MNRAS, 486, 2995
Malhan, K., Valluri, M., & Freese, K. 2021, MNRAS, 501, 179
Massari, D., Koppelman, H. H., & Helmi, A. 2019, A&A, 630, L4
McConnachie, A. W., & Côté, P. 2010, ApJL, 722, L209
Miyamoto, M., & Nagai, R. 1975, PASJ, 27, 533
Nadler, E. O., Drlica-Wagner, A., Bechtol, K., et al. 2021, PhrRvL, 126, 091101
Naidu, R. P., Conroy, C., Bonaca, A., et al. 2020, ApJ, 901, 48
Navarro, J. F., Frenk, C. S., & White, S. D. 1997, ApJ, 490, 493
Price-Whelan, A. M. 2017, JOSS, 2, 388
Price-Whelan, A. M., & Bonaca, A. 2018, ApJL, 863, L20
Price-Whelan, A. M., Sipócz, B. M., Günther, H. M., et al. 2018, AJ, 156, 123
Simon, J. D., & Geha, M. 2007, ApJ, 670, 313
Spitzer, L. 1987, Dynamical Evolution of Globular Clusters (Princeton, NJ: Princeton Univ. Press)
Springel, V., Wang, J., Vogelsberger, M., et al. 2008, MNRAS, 391, 1685
Virtanen, P., Gommers, R., Oliphant, T. E., et al. 2020, NatMe, 17, 261
Walt, S. v. d., Colbert, S. C., & Varoquaux, G. 2011, CSE, 13, 22
Webb, J. J., & Bovy, J. 2019, MNRAS, 485, 5929
Yoon, J. H., Johnston, K. V., & Hogg, D. W. 2011, ApJ, 731, 58